# APTAMER-BASED BIOSENSOR FOR PLATELET-DERIVED GROWTH FACTOR-BB USING FLUORESCENCE RESONANCE ENERGY TRANSFER

by

Cally A. Moore, B.S.

A thesis submitted to the Graduate Council of
Texas State University in partial fulfillment
of the requirements for the Degree of
Master of Science
with a Major in Biochemistry
May 2017

Committee Members:

Tania Betancourt, Chair

Kevin Lewis

Shannon Weigum

## FAIR USE AND AUTHOR'S PERMISSION STATEMENT



### Duplication Permission

## ACKNOWLEDGEMENTS

Foremost, I would like to express my sincere gratitude towards my advisor Dr. Tania Betancourt for her continued support of my work and for her patience, motivation, enthusiasm, and immense knowledge. Besides my advisor I would like to thank the rest of my thesis committee, Dr. Kevin Lewis and Dr. Shannon Weigum, for their encouragement, insightful comments, and hard questions. This work would not have been possible without the lab space and equipment that they both generously provided. I also thank my fellow lab mates for the stimulating discussions and support.

In particular, I would like to thank Elizabeth McIvor and Janet Vela Ross for their constant inspiration and encouragement through difficult times. Last but not least I would like to thank my mother, father, sister and Layla for supporting me through this endeavor.

## TABLE OF CONTENTS

**Page**

## LIST OF TABLES

**Table** **Page**

## LIST OF FIGURES

**Figure** **Page**

## LIST OF FIGURES

**Figure** **Page**

# I. INTRODUCTION

## 1.1 IMAGE-GUIDED THERAPY

Image-guided therapy is an emerging therapeutic strategy that utilizes information about the diseased tissue gathered through a bioimaging technique to direct localized therapies including but not limited to drug delivery, tissue ablation, or surgical resection (1). An example of image-guided therapy is radiofrequency ablation (RFA) in which the placement of an electrode in a patient is monitored with imaging, such as computed tomography (CT). At the desired location, current is passed through the electrode to generate heat, such that only the targeted tissue is ablated (2, 3). Another example of image-guided therapy is laser ablation, in which a near-infrared laser beam is directed to the target treatment site with the aid of endoscopy (2, 3).

Targeted anticancer therapies aim to address the downfalls of current cancer treatment strategies that rely on systemic administration of chemotherapeutic agents. Conventional drug delivery, including that of anticancer agents, is inherently flawed in that it is based upon absorption of the drug across biological membranes (4). This requires high dosages of the drug to be administered in order to achieve the therapeutic concentrations necessary at the site of the disease. This, in turn, results in significant toxicity to healthy tissues. Targeted drug delivery is a method of drug delivery, established predominantly in nanomedicine, that aims to increase the concentration of drug that reaches the diseased site, while minimizing exposure of healthy tissues and thereby reducing adverse side-effects (4, 5). The ultimate aim of targeted drug delivery is to both localize and prolong interaction between the drug and diseased tissue.

Image-guided therapies for localized cancer treatment rely on the use of theranostic agents that combine capabilities for diagnosis and therapy into a single system. Theranostic agents are typically designed to include a biosensing mechanism that is able to provide a signal upon recognition of a characteristic molecular or physiochemical feature of the diseased tissue, as well as a mechanism for imparting localized anti-cancer activity following molecular recognition of the target site. There are a variety of biosensing systems that can be utilized in theranostic nanomaterials. Such systems include quantum dots, small particles with finely tunable optoelectronic properties, and aptamer-based fluorescence probes that utilize Förster resonance energy transfer, FRET (6). Aptamers are short, single-stranded oligonucleotides that bind a target molecule with high affinity (7). Identification of aptamers is done through an *in vitro* process known as systematic evolution of ligands by exponential enrichment (SELEX) (7). The ability of aptamers to bind their target molecule with high affinity has made them ideal for use in nanomaterials as sensing systems.

The integration of aptamers into nanomaterials produces highly selective and sensitive molecular recognition sensors. Aptamer probes for molecular sensing have two general requirements: 1) Recognition of target molecule with high affinity, high specificity, rapid response time, and stability. This generates a stable sensor with low detection limits and low interference. 2) Production of a physically detectable signal, such as fluorescence, upon binding to the target molecule (8). The use of aptamer-functionalized nanomaterials has been widely employed in drug-delivery systems (9-11). In these systems, aptamers decorated on the surface of the nanomaterial act as targeting agents that mediate specific recognition and binding of the nanomaterial to molecular

targets. Aptamer-based FRET sensors have also often been attached to nanomaterials as a means to both direct the nanomaterial to the target as well as to visualize binding to that target. Using an aptamer-based sensing system to target a disease biomarker, such as proteins overexpressed in cancers, allows for detectability of the diseased site to target drug release. The focus of the work described in this thesis is the development of an aptamer-based FRET sensor that could be utilized as the biorecognition element of an image-guided nanocarrier for tumor-specific drug delivery.

## 1.2 PLATELET-DERIVED GROWTH FACTOR BB

Platelet-derived growth factor, PDGF, is a dimeric glycoprotein comprised of two subunits, A and B, which may assemble as the homodimers, -AA, -BB, or the heterodimer, -AB. Platelet-derived growth factor receptor, PDGFR, is a cell surface tyrosine kinase receptor that exists in two isoforms, alpha, α, and beta, β (12). Dimerization of the receptor upon PDGF binding activates the kinase activity of PDGFR. This dimerization leads to three possible receptor arrangements, -αα, -ββ, and -αβ. PDGF-AA binds only to the PDGFR-αα isoform, while PDGF-AB can bind both PDGFR-αα and PDGFR-αβ isoforms (12-14). Platelet-derived growth factor BB, PDGF-BB, is a member of a growth factor family that stimulates autocrine growth and angiogenesis, or the formation of new blood vessels from existing tissue (15). PDGF-BB is the only dimeric unit that can bind all three receptor arrangements, PDGFR-αα, PDGFR-ββ, and PDGFR-αβ (12-15). The selective binding of PDGF subunits makes the PDGF/PDGFR system highly adaptable.

Signaling for PDGF by PDGFR is highly regulated and carefully controlled. Tight

regulation of PDGF expression in healthy tissues is critical given PDGF's functionality; PDGF isoforms stimulate cell growth, proliferation, mobility of mesenchymal cells, and angiogenesis, the formation of new blood vessels from preexisting vasculature (15-17). PDGF is expressed beginning in early embryonic development and is continued throughout adult life. In adults, PDGF signaling promotes wound healing by stimulating fibroblasts, smooth muscle, and inflammatory cells (15, 16). In mice, previous knockout studies of both PDGF-A and PDGF-B have proved to be lethal for the developing embryo (16). Lethality before embryonic day ten, or premature death shortly after birth was seen with PDGF-A knockout, and lethality in the latter stages of embryonic development was observed with PDGF-B knockout (16). Histological studies of the PDGF-A-deficient tissues revealed defective pulmonary alveoli development, mesenchymal stem cell defects, and reduced brain oligodendrocytes (16). Lethality of PDGF-B deficient mice was found to be caused by migration failure of the pericyte to new blood vessels. Abnormal pericyte migration leads to abnormal blood vessel formation and defective development of the cardiovascular system (16).

Overexpression of PDGF is associated with many diseases, all of which are distinguished by excessive cell proliferation, such as fibrosis and cancer (15,16). The overexpression of PDGF has been documented in several different cancers including breast, ovarian, myelomonocytic leukemia, osteosarcoma, neurofibroma, and glioma (14, 19-23). High levels of PDGF in cancer tissue are indicative of an autocrine neoplastic mechanism. Extracellular matrix production and myofibroblast-like cell proliferation, a desmoplastic response of breast carcinoma cells, is PDGF-dependent (18-22). The overexpression of PDGF has made it a biomarker for cancer, and thus, a highly utilizable

target molecule in aptamer-based sensing systems used in drug delivery. *In vitro* studies with a mesangioproliferative glomerulonephritis rat model utilizing a PEG-modified anti-PDGF-B aptamer exhibited a 64% decrease in mitosis, 95% decrease in mesangial cell proliferation, and 33.5% reduction of interstitial fluid pressure, IFP, from 14.6 mm Hg to 9.7 mm Hg (25). Further studies utilized PDGF-BB protein as a targeting agent to increase cellular uptake of drug-loaded nanoparticles (25, 26). When PDGF-BB was attached to the surface of biodegradable nanoparticles containing dexamethasone, cellular uptake was increased while cell proliferation was decreased (32). In another study, a fluorophore-functionalized PDGF-BB aptamer and its quencher-functionalized partial-complement were conjugated to a silver nanoparticle for fluorescence resonance energy transfer (FRET) detection of PDGF-BB binding (24). This study shed light on the abilities of PDGF-BB aptamer-functionalized nanoparticles to generate an optical signal upon target binding.

## 1.3 APTAMER-ENABLED DRUG DELIVERY SYSTEMS

Micelles are used in stimuli responsive drug delivery systems because of their flexibility for design, small size, high stability, and avoidance of rapid renal elimination as compared to conventional drug solutions (8). The use of stimuli-responsive micellar systems enables dosage-controlled drug delivery systems that are temporal and uniform in release (8, 12, 25, 31, 32). In our group, the development of photoresponsive micelles as theranostic agents for image-guided drug delivery is being pursued. Such photo-responsive micelles can be designed to integrate surface FRET sensors as a means to signal interaction of the micelle with the targeted tumors. As envisioned, the optical

signal from the FRET sensor can then be utilized by a user (e.g. a clinician) to initiate externally controlled laser-induced disruption of the photoresponsive micelles, leading to drug delivery. The efficiency of energy transfer in FRET is dependent upon the distance between the donor and the acceptor, and is directly proportional the sixth power of the distance between the two molecules, known as the Förster radius, 10-100 Å (13, 29, 31).

A FRET sensor that utilized a PDGF-BB aptamer complex functionalized on the surface of metal nanoparticles was recently reported for the detection of PDGF-BB (24). This study aimed to optimize and investigate the capabilities of a FRET sensor that utilized an aptamer complex (prepared from a fluorophore-functionalized PDGF-BB aptamer and its quencher-functionalized partial complement) bound to silver and gold nanoparticles (24). When the fluorophore-functionalized PDGF-BB aptamer was hybridized with its quencher-functionalized partial complement, the two probes would come within the Förster radius, thereby enabling the quencher to act as an acceptor of fluorophore energy transfer and thus preventing fluorophore emission. The FRET sensor described in this prior work was designed such that when the PDGF-BB aptamer binds to its target, PDGF-BB, the quencher strand is displaced (24). This displacement results in an increasing distance, outside the Förster radius, between the two probes and results in detectable emission of the fluorophore (24).

## 1.4 OVERALL RESEARCH PROJECT

In this work, we optimized the previously reported (24) FRET sensor for the detection of PDGF-BB by investigating the effect of probe oligonucleotide sequence, stability, and ability to form appropriate secondary structure for target recognition. Specifically, in the sensors investigated, the PDGF-BB aptamer is functionalized with a fluorophore and a partial complement to the aptamer is functionalized with a quencher. When the two are hybridized, little fluorescence is detectable due to FRET between the fluorophore and quencher. When the fluorophore-functionalized aptamer binds to its PDGF-BB target, the quencher-functionalized partial complement is displaced, allowing for a detectable fluorescence signal, as illustrated in **Fig 1A.**

While the previously reported PDGF-BB aptamer-based FRET system (24) showed up to a three-fold increase in fluorescence when the aptamer system was exposed to PDGF-BB as compared to BSA, our own investigation revealed that in this system only a fraction of the potential fluorescence development (dehybridization-induced fluorescence rise) was achieved upon PDGF-BB exposure. This led to the redesign of the current aptamer-based FRET system with five new systems, shown in **Fig. 1B**. This work compares the sensitivity, efficacy, and selectivity of each newly designed PDGF-BB aptamer-based FRET sensor (Systems 2 through 6) to the previously used system, System 1.

**A**

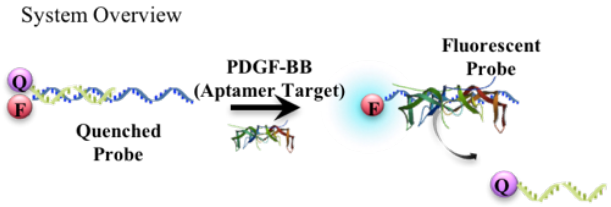


**B**

| | | | |
|---|---|---|---|
| **Fluorophore 1** (F1) | **5'** | FAM6 | **CAG GCT ACG GCA** CGT AGA GCA TCA CCA TGA TCC TG$(A)_{18}$ 3' |
| **System 1** (Q1) | 3' | BHQ1 | **GTC CGA TGC CGT** 5' |
| **System 2** (Q2) | 3' | BHQ1 | **GTC CAA TGC CG** 5' |
| **System 3** (Q3) | 3' | BHQ1 | **GTC CGA TGC C** 5' |
| **System 4** (Q4) | 3' A | BHQ1 | **GTC CGA TGC** 5' |
| **System 5** (Q5) | 3' A AAA | BHQ1 | **GTC CGA** 5' |
| **Fluorophore 2** (F2) | **5'** | FAM6 | CAT TA**C AGG CTA** CGG CAC GTA GAG CAT CAC CAT GAT CCT G$(A)_{18}$ 3' |
| **System 6** (Q6) | 3' | BHQ1 | GTA AT**G TCG GAT** 5' |

Figure 1(A). Schematic representation of the aptamer-based FRET sensor. Upon exposure of the hybridized complex to PDGF-BB, the quencher-functionalized partial complement becomes displaced leading to an increase in fluorescent signal. (B). Oligonucleotide sequences used in Systems 1−6 for detection of PDGF-BB. PDGF-BB aptamer-containing strands, **F1** and **F2**, are shown in the 5'–3' direction while **Quenchers 1-6** (Q1-Q6) are shown in the 3'–5' direction to illustrate binding of the partially complementary quenching strands to the aptamer. Bolded sequences indicate nucleotides that bind to the aptamer region of the F strands. Sequences underlined represent nonspecific nucleotide extensions and their complements.

For each system, we examined the thermal stability by conducting melting curve analysis to indicate complexed system viability at physiological temperatures, response to PDGF-BB as a function of concentration, and PDGF-BB selectivity by comparing the fluorescence enhancement of the systems when exposed to other commonly found proteins. We also utilized electrophoretic mobility gel shift assays, EMSAs, to further show the binding ability of each system to PDGF-BB. Ultimately, our work implies the design of a new aptamer-based FRET sensor for PDGF-BB that is more selective, responsive, and efficient than the previously reported one.

# II. MATERIALS AND METHODS

## 2.1 SYSTEM DESIGN

Several two-stranded oligonucleotide systems were investigated as FRET-enabled sensors for the detection of platelet-derived growth factor-BB, PDGF-BB. These systems utilized the anti-PDGF-BB aptamer sequence, **5**' **CAGGCTACGGCACGTAGAG CATCACCATGATCCTGA** 3**'**, originally identified by Green *et al.* (35) and reported by Li *et al.* as a PDGF-BB aptamer-based FRET sensor (24). Oligonucleotides were prepared by solid phase synthesis by Integrated DNA Technologies (Coralville, IA, USA). Oligonucleotide sequences for the six systems examined in this study are listed in **Fig. 1** (Chapter I). In these sequences, F1 and F2 strands consist of modified anti-PDGF-BB aptamer sequence that have been labeled on their 5' end with 6-carboxyfluorescein (FAM6). Both F1 and F2 strands include an 18-nt polyA tail that is designed to enable later use of these sequences in biosensing nanomaterials. Strands Q1–Q6 refer to strands that are partially complementary to F1 and F2 and that are functionalized with Black Hole Quencher® 1 (BHQ1). The hybridized complements of F1 with Q1–Q5 or of F2 with Q6 form Systems 1-6 as shown in **Fig. 1**. For brevity, the following nomenclature will be used to refer to the complements formed by hybridization of the following strand pairs: **System 1:** F1 + Q1, **System 2**: F1 + Q2, **System 3**: F1 + Q3, **System 4**: F1 + Q4, **System 5**: F1 + Q5, **System 6**: F2 + Q6.

The systems studied in this research (**Fig. 1**), were designed based on the original PDGF-BB FRET sensor, System 1, reported by Li *et al.* (24). The initial use of System 1 was selected because of an alternate, tangential project within the lab in which PDGF-

responsive DNA complements will be utilized as part of a stimuli-responsive nanomedicine system. Systems 2–6, which were the focus of the work described in this thesis, were developed as a way to enhance the sensitivity of the PDGF-BB FRET sensor.

Systems 2−5 were designed on the rationale that reducing the number of aptamer nucleotides hybridized to its partial complement would allow the aptamer to form its necessary secondary structure more readily, thereby enabling improved interaction with the target and more efficient displacement of the partial complement upon PDGF-BB binding. System 2 contains one non-complimentary nucleotide that replaces a G-C pair with a mismatched base pair. This was done to further reduce the stability of System 2 allowing for easier displacement of the partial complement upon PDGF-BB exposure. The additional "A" nucleotides on the 3' end of Systems 4 and 5 were added to elongate the strand to 10 nt, which is the minimum number of nucleotides required for solid phase synthesis. The identity of these added nucleotides, namely "A" strands, were selected to avoid the formation of undesired hairpin structures, self-hybrids, or other undesired complements. The thermodynamics, mainly the melting temperature for each system, was also considered in their selection.

System 6 was designed based on work done by Nutiu and Li (31) who developed fluorescent aptamer sensors for the detection of the target molecules adenosine and thrombin. In their work, a nonspecific 5-nt sequence, CACGT, was added between an aptamer motif and a non-specific binding domain for a partially complementary 12-nt quencher-functionalized strand to bind the new 5-nt and 7-nt of the aptamer. We used this rationale, along with thermodynamic properties such as dimer formation and melting temperature, to create the second fluorophore-functionalized PDGF-BB aptamer-

containing strand, F2, containing 5 nonspecific nucleotides, CATTA, on the 5' end. In the previously reported PDGF-BB aptamer-based FRET sensor (24), System 1, binding of the 12 nt partial complement to the PDGF-BB aptamer inhibits formation of the first stem loop. Using this as a starting point, Systems 2-6 were designed to improve the sensitivity and effectiveness of the sensor by increasing their responsiveness to PDGF-BB. To optimize the FRET sensor design, the structure of the PDFG-BB aptamer was first considered. The PDGF-BB aptamer is 35 nt in length. The predicted secondary hairpin structure of the 53 nt and 58 nt aptamer-containing strands F1 and F2 (including the polyA tails) are shown in **Fig. 2**. The fluorophore, FAM6, is positioned on the 5' end of the PDGF-BB aptamer and the quencher, BHQ1, is positioned at the 3' end of the partial complements. The quencher-functionalized partial complements bind to the first 12 nt of the aptamer sequence. Binding of these first 12 nt prevents the aptamer from forming the first stem-loop necessary for PDGF-BB recognition and binding. Systems 2-5 were designed to minimize the partial complement binding in the stem-loop forming nucleotides while maintaining the necessary number of nucleotides for solid-phase synthesis and overall stability. System 6 was designed with the same intention; however, System 6, contains five additional nucleotides on the 5' end of the PDGF-BB aptamer, and thus their complements were added to the 3' end of the partial complement. These five nucleotides were chosen as they did not interfere with the secondary structure formation of the aptamer needed for PDGF-BB binding. Integrated DNA Technologies OligoAnalyzer tool was used to determine melting temperature and hairpin formation likelihood when choosing the five additional nucleotides. Conditions under which the $T_m$ values and secondary structures were predicted and calculated using the IDT

OligoAnalyzer tool were as follows: 25 nM oligonucleotide concentration and 157 mM $Na^+$ concentration (34).

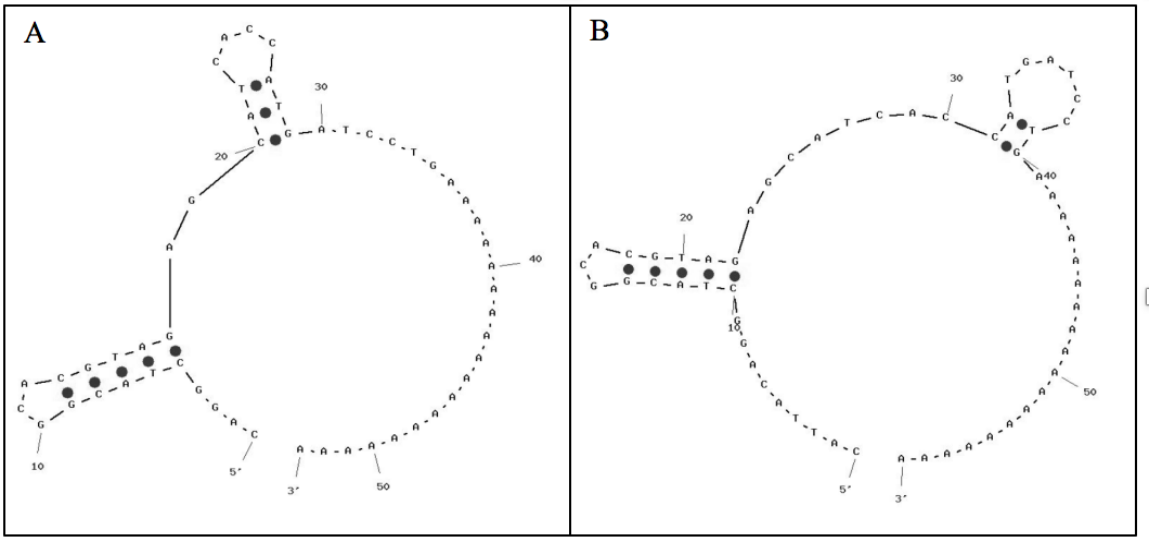


Figure 2(A) Secondary structure predicted using IDT OligoAnalyzer tool for PDGF-BB aptamer 1, F1, and (B) PDGF-BB aptamer with additional five nucleotides, F2 (27).

6-carboxyfluorescein, FAM-6, was chosen as the fluorophore for all systems because of its ubiquitous use in molecular beacons. Black Hole Quencher®-1, BHQ1, was chosen over the commonly used FAM6/Tam (FAM6 and Tamra) FRET pair because of the exceptional spectral overlap between Tamra and FAM-6 and its high extinction coefficient, as shown in **Fig. 3**.

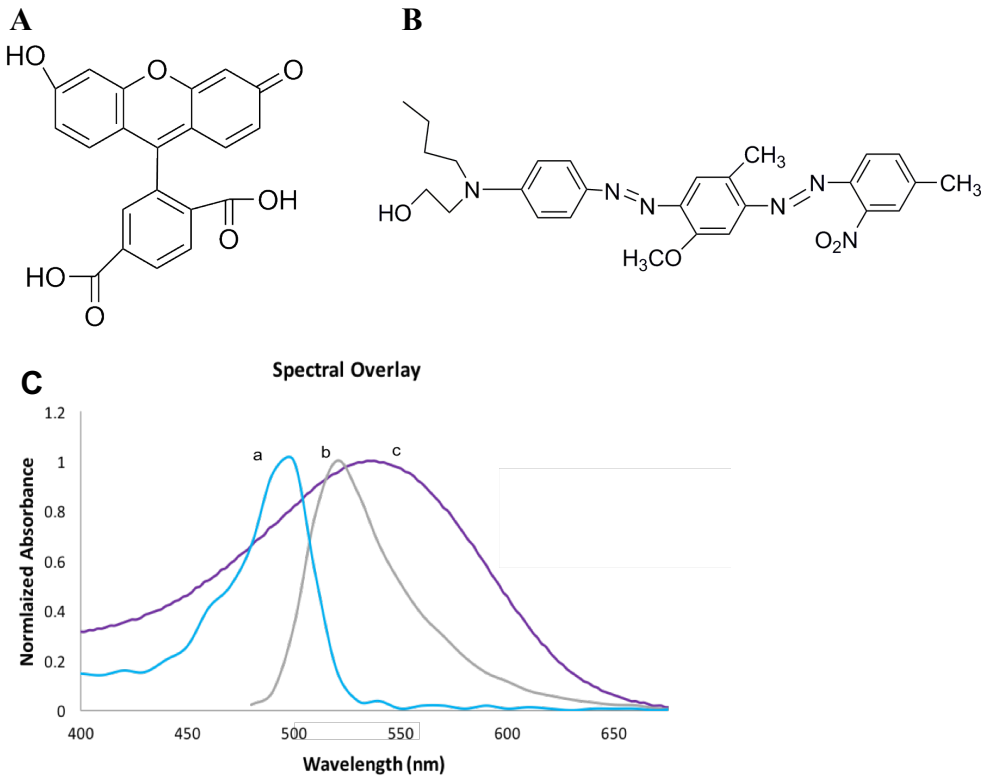


| D | Extinction Coefficient (L $mol^{-1}$ $cm^{-1}$ | Absorbance Maximum | Emission Maximum | Molecular Weight (g/mol) |
|---|---|---|---|---|
| 6- Carboxyfluorescein FAM6 | 20960 | 495 nm | 520 nm | 537.5 |
| Black Hole Quencher-1 BHQ1 | 8000 | 534 nm | -- | 554.5 |

Figure 3(A) Structure of 6-carboxyfluorescein, FAM-6 (B) Structure of Black Hole Quencher-1, BHQ1. (C) The normalized spectral overlap of FAM6 and BHQ1 (a: FAM6 absorption, b: FAM6 fluorescence, c: BHQ1 absorption. (D) Molar extinction coefficients, absorbance maximum, emission maximum, and molecular weight of FAM-6 and BHQ1 (27).

## 2.2 THERMAL STUDIES

Thermal studies were performed to demonstrate hybridization of each system, investigate hybrid stability at room and physiological temperatures, and determine the melting temperature for each system. All thermal studies were performed using a Cary Eclipse fluorescence spectrophotometer from Agilent Technologies (Santa Clara, CA). All thermal studies were conducted in sterile 1x PBS (0.01 M phosphate buffer, 0.150 M sodium chloride), pH 7.4. Samples were not pre-hybridized; instead, they were heated and cooled at 1 °C per min for 3 thermal cycles. A thermal cycle consisted of heating from 5 °C to 95 °C, pausing for 5 min a 95 °C, cooling back down to 5 °C, and pausing at 5 °C for 5 min. The first cycle was considered the hybridization cycle, the second cycle was used to calculate the melting temperatures, and the third cycle was used to determine further stability of each system and replication of the thermal behavior of cycle 2. Oligonucleotide solutions with final concentration of 25 nM for both the F and Q strands were used in these studies. Sample temperatures were monitored using the internal probe from the Cary Eclipse. Fluorescence readings were taken every 1 °C ($\lambda_{Ex}$ = 495 nm, $\lambda_{Em}$ = 521 nm). The melting temperature for each system was determined using the auto calculation feature on the Cary Eclipse via the first derivative method. Calculated melting temperatures were then compared to the predicted melting temperature obtained from the OligoAnalyzer® Tool (IDT, Coralville, IA, USA).

## 2.3 INVESTIGATION OF SYSTEM RESPONSE TO PDGF-BB VIA FLUORESCENCE STUDIES

To determine response of each system to PDGF-BB, fluorescence was monitored using a Biotek Synergy H4 Multi-Mode Plate Reader from Biotek Instruments, Inc. (Winooski, VT, USA). PDGF-BB was obtained from R&D Systems, Inc. (Minneapolis, MN, USA) and dissolved in a solution containing 4 mM HCl and 1 mg/mL bovine serum albumin (BSA, Sigma-Aldrich, St. Louis, MO, USA). Further PDGF dilutions were prepared in 1 mg/mL BSA solution as suggested previously (24) to enhance protein stability and also provide a background of nonspecific protein. Samples were prepared to a final concentration of 25 nM for both the F strand and the Q strand, when applicable. Samples were hybridized by heating to 95 °C for 5−10 min using an Eppendorf ThermoMixer® (Eppendorf, Hamburg, Germany), and cooling to room temperature overnight. Following hybridization, 20 μL of each sample were placed into the wells of a 384-well plate in triplicate. Then, 20 μL of either 1 mg/mL (10 μM) BSA or 1000 ng/mL (40.65 nM) PDGF (which contained 1 mg/mL BSA) was added to the samples. This resulted in the following final concentrations in each well: 25 nM F and Q, and either 40.65 nM of PDGF-BB (including 1 mg/mL BSA) or only 40.65 nM (0.02 mg/mL) BSA without PDGF-BB. The concentration of PDGF-BB was chosen based on the studies performed by Li *et al.* 2013 (24). Using the Biotek Synergy H4, fluorescence readings were taken ($\lambda_{Ex}$ = 495 nm, $\lambda_{Em}$ = 521 nm).

Data was processed for each system by calculating the $F/F_0$ ratio defined by Equation 1: $F/F_0 = \frac{Fluorescense\ \ response\ to\ \ PDGF-BB}{Fluroescence\ response\ to\ BSA}$ (24).

The value of $F/F_0$ is indicative of the overall fold increase in fluorescence when the

aptamer system is exposed to PDGF-BB compared to a control protein, BSA. In addition to $F/F_0$, percentage of unquenched F before and after the addition of PDGF-BB as compared to the control, BSA, was also used as a means to determine the level of response of the sensor. Data from replicate samples were averaged, their standard deviation determined, and any statistical analysis was performed using a two-tailed t-test in excel.

## 2.4 ELECTROPHORETIC MOBILITY SHIFT ASSAY FOR PDGF-BB APTAMER BINDING

To visualize binding of the aptamer to PDGF-BB, and thus further confirm displacement of the quenching strand upon PDGF binding, electrophoretic mobility shift assays, EMSA, were performed. Protein-DNA interactions are studied using this technique because different conformations and stoichiometric ratios can be resolved. This allows for the qualitative identification of a specific DNA sequence binding a target protein. EMSAs were performed using 1.0 mm, 15-well Novex™ Value™ 4-20% poly(acrylamide) Tris-Glycine Mini Polyacrylamide Gels, XCell Surelock® Mini Cell, and Thermo Scientific Owl® EC-105 Compact Electrophoresis Power Supply System (120 V) from ThermoFisher Scientific (Waltham, MA, USA).

Oligonucleotide samples were prepared at 20-fold the concentration used in the fluorescence studies described below (**Fig. 5)** to allow for enough sample to visualize on the gel. Solutions of F1, F2, and Systems 1–6 were (at a 1:1 molar ratio of F:Q strands) were prepared at an oligonucleotide concentration of 500 nM. In addition, 813 nM BSA and 813 nM PDGF-BB were added as appropriately. ESMAs were run using 1x Tris-

glycine (1xTG) buffer (0.025 M Tris, 0.192 M glycine, pH 8.3). Loading dye was comprised of 1x PBS, 15% glycerol, and bromophenol blue. Gels were run for 1.5 – 2.5 h at 75 – 85 V. Further gel specifications for time and voltage are provided in the respective figure descriptions. Gels were then imaged for fluorescence using a PharosFX™ Imager obtained from Bio-Rad Laboratories (Hercules, CA, USA). Following fluorescence imaging, gels were stained using colloidal Commassie stain prepared in-house which contained 10% ammonium sulfate, 0.1% Commassie G-250, 3% ortho-phosphoric acid, and 20% ethanol. All reagents for the colloidal Commassie stain were obtained from Sigma-Aldrich (St. Louis, MO, USA) except for the Commassie brilliant blue G-250 which was obtained from ThermoFisher Scientific (Waltham, MA, USA). Gels were stained for a minimum of 12 h and a maximum of 16 h to ensure full staining of the samples. Gels were then imaged before they were de-stained using an in-house de-stain solution comprised of 10% ammonium sulfate, 3% ortho-phosphoric acid, and 20% ethanol for 12 h. Following de-stain, gels were imaged again. Images were taken post de-stain to provide a picture with low background, yet visible bands. All images for colloidal Commassie stain were taken using the ChemiDoc XRS+ System from Bio-Rad Laboratories (Hercules, CA, USA).

## 2.5 SENSOR SENSITIVITY TO PDGF-BB

Oligonucleotide hybrids were prepared at a 1:1 molar ratio of the respective F and Q strands in 1x PBS, 1 mg/mL BSA. Samples were hybridized following the same protocol described for the fluorescence studies: hybridization at 95 °C for 10 min followed by cooling to room temperature. Using a constant oligonucleotide concentration of 25 nM, F1, F2, and Systems 1–6 were exposed to varying PDGF-BB concentrations,

250 ng/mL – 3.9 ng/mL, to investigate the sensitivity of each system to the target molecule. The molar ratios between PDGF-BB and the aptamer sensor are shown in **Table 1**. The most promising systems, Systems 1 and 6, were also exposed to 500 ng/mL (20.32 nM) PDGF-BB. 384 microwell plates were utilized by preparing the oligonucleotides and PDGF-BB at 2x the final concentration. Equal volumes of each, oligonucleotide + PDGF-BB, were added to the 384 microwell plate to quantify the fluorescence signal.

**Table 1.** Concentrations of PDGF-BB and aptamer sensor used to determine the sensitivity of the aptamer sensor to PDGF-BB. Concentrations of the target protein are shown in both ng/mL and nM. The molar ratio of PDGF-BB to the aptamer sensor (PDGF-BB:DNA aptamer) is also reported.

| System Concentration (nM) | PDGF-BB (ng/mL) | PDGF-BB (nM) | Molar Ratio of PDGF-BB:System |
|---|---|---|---|
| **25** | 500 | 20.32 | 0.82 |
| **25** | 250 | 10.16 | 0.41 |
| **25** | 125 | 5.08 | 0.20 |
| **25** | 62.5 | 2.54 | 0.10 |
| **25** | 31.2 | 1.27 | 0.05 |
| **25** | 15.6 | 0.64 | 0.03 |
| **25** | 7.8 | 0.32 | 0.01 |
| **25** | 3.9 | 0.16 | 0.005 |

## 2.6 SENSOR SELECTIVITY

Oligonucleotide hybrids were prepared at a 1:1 molar ratio of the respective F and Q strands. Samples were hybridized following the same protocol described for the fluorescence and sensitivity studies: denaturation at 95 °C for 10 min followed by cooling to room temperature. Using a constant oligonucleotide concentration of 25 nM, F1, F2,

and Systems 1–6 were exposed to 1000 ng/mL of vascular endothelial growth factor (VEGF), 1000 ng/mL PDGF-BB, 1% Fetal Bovine Serum (FBS), 1% FBS + PDGF-BB, or 1000 ng/mL BSA. This was done to investigate the selectivity of each system towards PDGF-BB and examine the effect of endogenous serum proteins on target binding. Studies were carried out as described above for PDGF-BB sensitivity: oligonucleotides and proteins were prepared at 2x the final concentration and added in equal volumes to the 384 microwell plate to quantify the fluorescence signal.

# III. RESULTS AND DISCUSSION

The overarching goal of this study was to optimize and enhance the currently used Platelet-Derived Growth Factor-BB (PDGF-BB) aptamer-based FRET sensor used for the detection of PDGF-BB. Specifically, we designed five additional PDGF-BB aptamer-based FRET sensors (Systems 1–5) to compare to the previously reported PDGF-BB-based FRET sensor (System 1). This research has developed an aptamer-based FRET sensor that generates a greater fluorescence signal upon PDGF-BB binding. The data collected in this research will contribute to the field of nanomedicine in the context of targeted drug-delivery systems, specifically aptamer-based targeted drug delivery systems.

## 3.1 SYSTEM DESIGN

Performing analysis on the oligonucleotide aptamer systems to determine hairpin and heterodimer formation, as well as a calculated melting temperature through the IDT OligoAnalyzer® Tool was a valuable tool in creating the five additional aptamer-based FRET sensors for PDGF-BB. The OligoAnalyzer® Tool has been established as a commonly utilized calculator for determining various oligonucleotide properties such as: melting temperature, hybridization, hairpin formation, heterodimer formation, molecular weight, extinction coefficient, effects of mismatches (33). This tool was used to design Systems 2–6 based on the predicted ΔG values for fluorophore strand and quenching strand hybridization, heterodimer and hairpin formation, and predicted melting temperatures. The predicted ΔG values and melting temperatures for Systems 1–6 are shown in **Table 2**.

**Table 2.** ΔG and $T_m$ values for Systems 16 as predicted by the OligoAnalyzer® Tool. $T_m$ values are predicted using the nearest neighbor model.
*$T_m$ values for Systems 4 and 5 were unable to be determined as these systems do not hybridize sufficiently in the temperature range studied.

| System | ΔG | $T_m$ Predicted | $T_m$ Determined |
|---|---|---|---|
| **1**: $F_1 + Q_1$ | -25.44 | 52.5 °C | 54.5 °C |
| **2**: $F_1 + Q_2$ | -14.08 | 44.4 °C | 46.9 °C |
| **3**: $F_1 + Q_3$ | -20.34 | 41.9 °C | 38.5 °C |
| **4**: $F_1 + Q_4$ | -17.27 | 34.8 °C | - |
| **5**: $F_1 + Q_5$ | -11.36 | 7.7 °C | - |
| **6**: $F_2 + Q_6$ | -20.00 | 40.0 °C | 42.5 °C |

Melting temperatures were determined using the fluorescence increase upon denaturation for each system. The results of the melting temperature studies are shown in **Fig. 4**. The temperature range used for melting temperature determination was 5 °C to 90 °C and fluorescence values were normalized based on the maximum fluorescence value of the respective unhybridized fluorophore-containing oligonucleotide strand present in the system, i.e. maximum fluorescence value of F1 for Systems 1-5 and F2 for System 6.

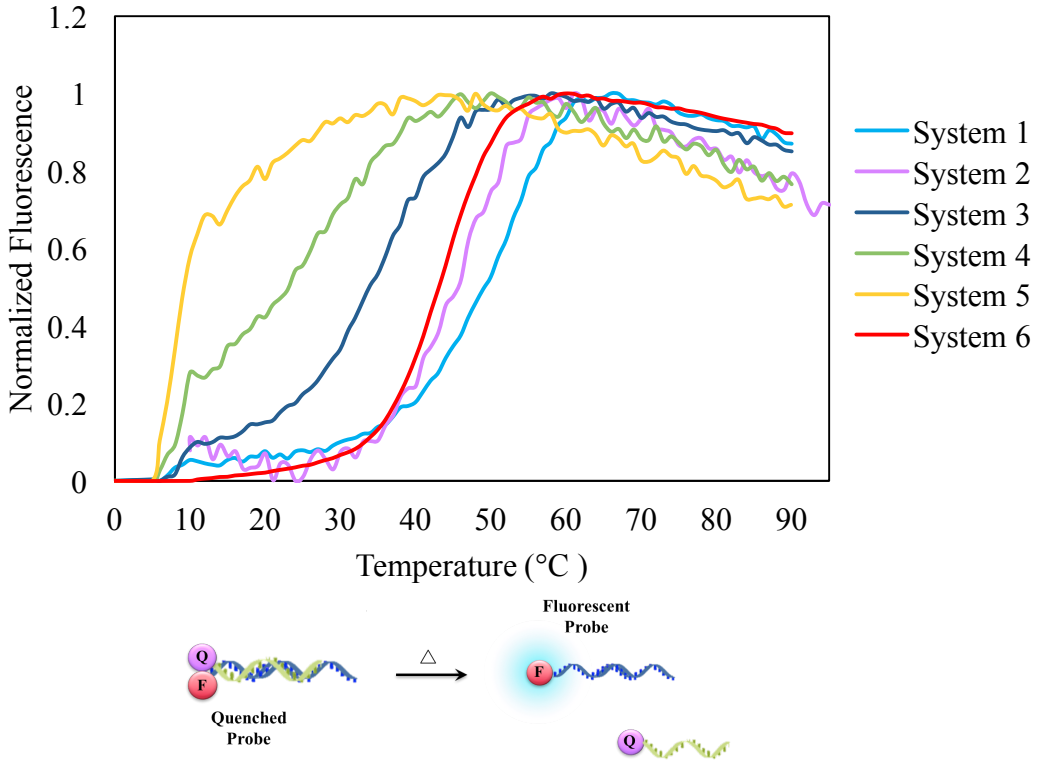


Figure 4. Melting temperatures for Systems 1–6 shown with normalized fluorescence. Melting temperatures were determined at 25 nM in 1x PBS for all systems. A schematic of dehybridization upon increasing temperature leading to an increase in fluorescence is shown below the graph.

Melting temperatures were calculated by taking the derivative of the fluorescence with respect to temperature and identifying the temperature at the maximum of the resultant $\partial A/\partial T$. The calculated melting temperatures for Systems 1–3 and System 6 are near that of the predicted melting temperatures. The melting temperature of systems 4 and 5 could not be determined experimentally due to the lack of overall hybridization stability at temperatures above 5–10 °C. Below 5 °C, the required temperature range to reach hybridization stability, system cooling results significant condensation outside of the cuvettes which prevents accurate data collection. In addition, running temperatures below 0 °C is not possible as it leads to sample freezing.

### 3.2 SYSTEM RESPONSE TO PDGF-BB

Systems 1–6, F1, and F2 were analyzed for responsiveness to PDGF-BB and BSA as the control. **Fig. 5** shows the response of Systems 1–6, F1, and F2 to both BSA (1 mg/mL) and PDGF-BB, 1000 ng/mL (40.65 nM). The ideal system would show low fluorescence values with the addition of BSA since the fluorophore and quenching strand would not have been displaced, and would show an increase in fluorescence to a value near that of its respective fluorophore strand, F1 or F2, upon interaction with PDGF-BB.

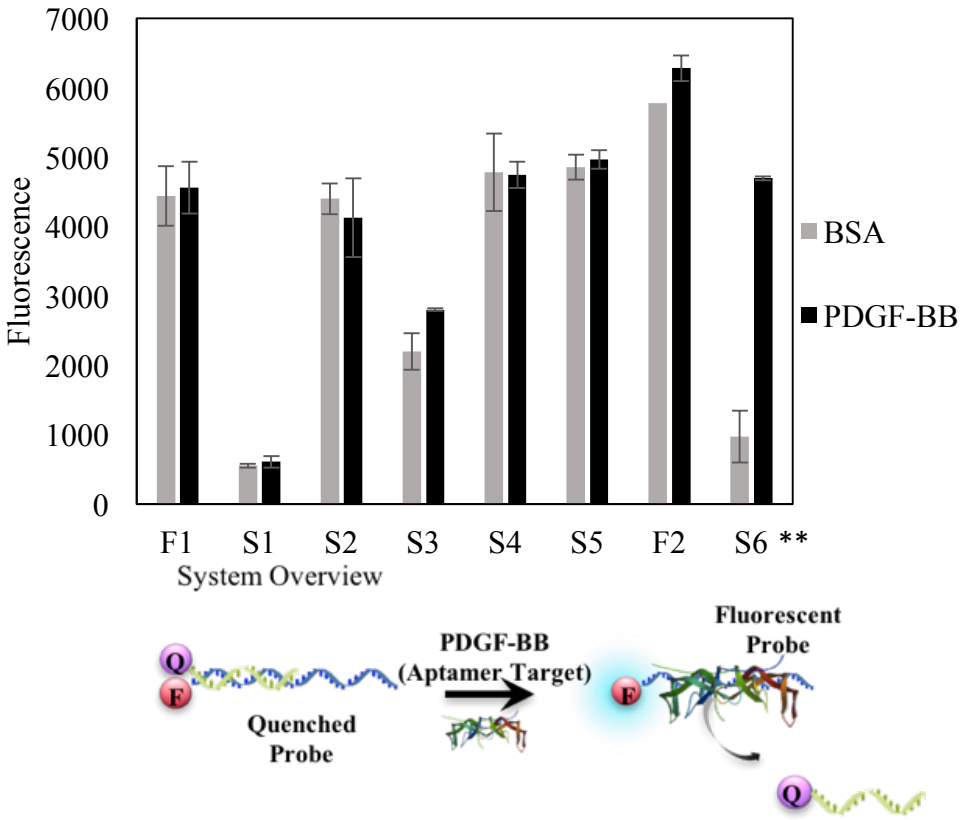


Figure 5. Response of Systems 1–6, F1, and F2 to 40.65 nM (1000 ng/mL) PDGF-BB, or 1 mg/mL BSA. A schematic of the partial-complement displacement upon PDGF-BB exposure leading to an increase in fluorescence is shown below the graph. The fluorescence values and standard deviations (n = 3) for each response are shown. All oligonucleotide strands in these samples were used at a concentration of 25 nM. $^{**}P \leq 0.01$.

As shown in **Fig. 5,** the fluorophore strands alone, F1 and F2, yield similar high fluorescence values when exposed to both BSA and PDGF-BB. Systems 2, 4, and 5 show little difference in the fluorescence values when PDGF-BB is added versus when BSA is added, indicating little to no hybridization at experimental conditions, and thereby no significant displacement of the quenching strand upon addition to PDGF-BB. System 1 while showing quenching due to the hybridization of the fluorophore strand to the quenching strand, does not show displacement of the quenching strand upon addition of PDGF-BB as the fluorescence values for both the addition of PDGF-BB and BSA are low. This most likely indicates that System 1 is too stable at experimental conditions to act as a sensor, i.e. System 1 is too stable at experimental conditions to bind to PDGF-BB and displace the partial complement. System 3 shows slight displacement with the addition of PDGF-BB over that of BSA as indicated by the lower fluorescence value of the BSA addition compared to that of the PDGF-BB addition. System 6 maintains hybridization in the presence of BSA, as indicated by the low fluorescence with BSA addition, and shows the highest increase in fluorescence upon addition of PDGF-BB.

The efficiency and sensitivity of the PDGF-BB FRET sensor has historically been reported as $F/F_0$, $\frac{Fluorescence\ intensity\ with\ PDGF-BB}{Fluroescence\ intensity\ with\ BSA}$ (24). $F/F_0$ reflects the increase in fluorescence, displacement of the quenching strand, after addition of the target protein, PDGF-BB, relative to the increase in fluorescence when BSA is added. When $F/F_0 = 1$, it implies no binding of the fluorophore-labeled strand, thus no displacement of the quencher-labeled strand, to PDGF-BB. When $F/F_0 > 1$ the quenching strand has been displaced from the aptamer, allowing for an increase in fluorescence, upon binding to PDGF-BB. **Fig. 6** shows the response ratio represented by $F/F_0$ increase, or fold increase,

for each system upon exposure to PDGF-BB.

As expected, the $F/F_0$ values for F1 and F2, the fluorophore strands alone, are near 1, indicating the same fluorescence values in the presence of both PDGF-BB and BSA. This is important as it reflects little to no fluorescence interference of the fluorophore-functionalized PDGF-BB aptamer when bound to its target protein, PDGF-BB. System 3 showed an $F/F_0$ value of 1.27, the highest of Systems 1-5, indicating some displacement of the quenching strand upon the addition of PDGF-BB. System 6 yielded the highest $F/F_0$ value of 4.84 indicating a large displacement of the quenching strand from the fluorophore-functionalized PDGF-BB aptamer. Time of 0 min refers to immediately after the addition of 1000 ng/mL PDGF-BB to 25 nM System 6.

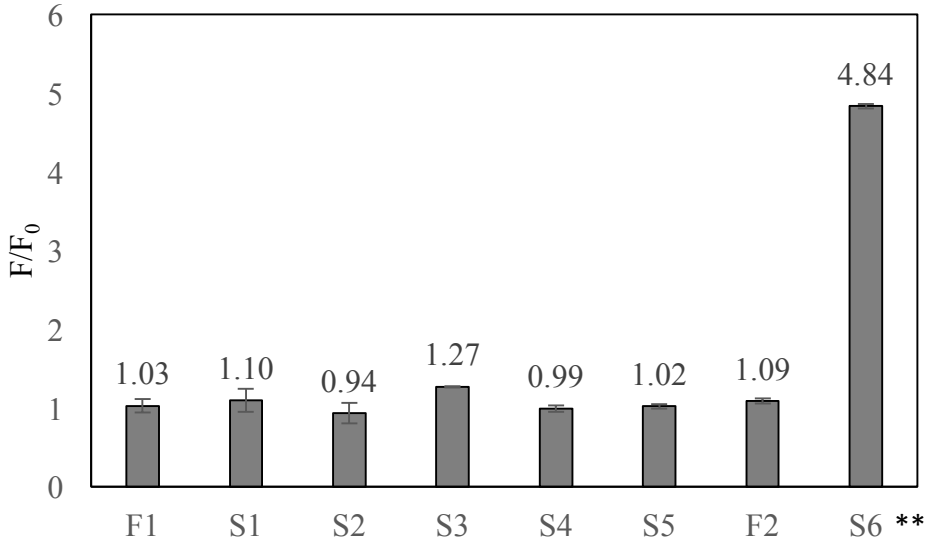


Figure 6. Response ratios for Systems 1–6, F1, and F2 (with each oligonucleotide strand at 25 nM) to PDGF-BB relative to that of BSA. PDGF-BB concentration was 40.65 nM (1000 ng/mL) and BSA concentration was 1 mg/mL. F/F0 represents the ratio of response relative to BSA, $\frac{Response\ to\ PDGF-BB}{Response\ to\ BSA}$. Error bars represent the standard deviation between replicates (n = 3). **P ≤ 0.01.

**Fig. 7** illustrates the stability of the F2 PDGF-BB aptamer bound to PDGF-BB over 90 min. The fluorescence values of the F2 PDGF-BB aptamer remain at a constant high value, compared to those of the sample exposed to BSA, indicating that F2 remains bound to PDGF-BB over 90 min. This is indicative of the high stability for the aptamer-protein complex, F2-PDGF-BB. Binding of the aptamer to PDGF-BB is immediate, as can be seen by the high increase in fluorescence immediately upon addition.

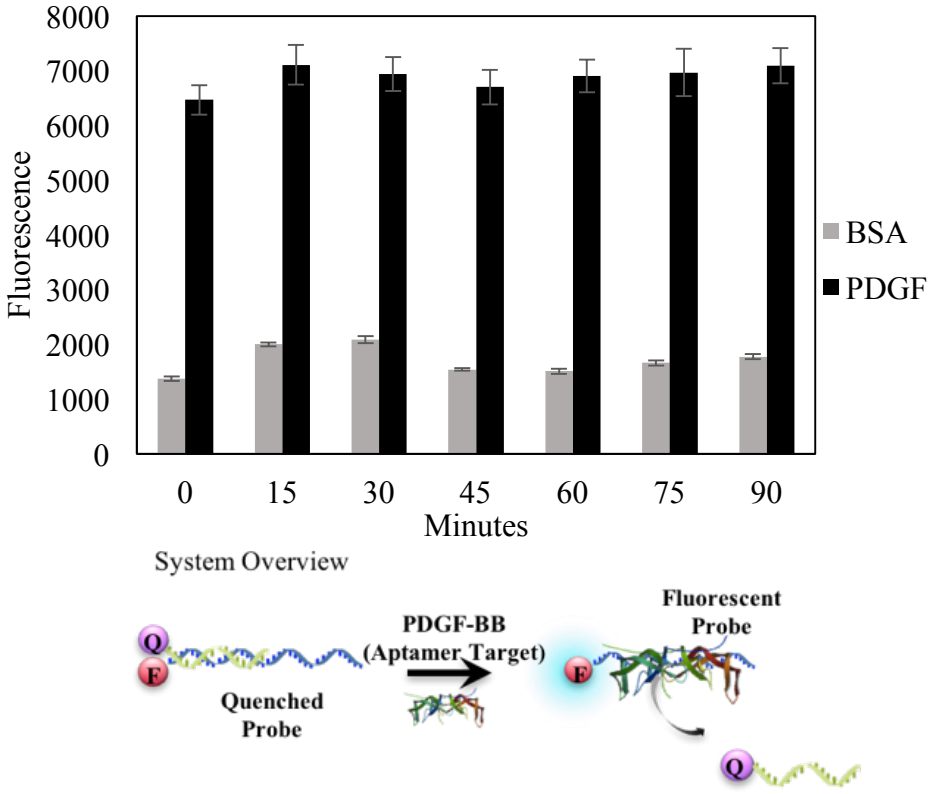


Figure 7. Displacement of System 6 with 1000 ng/mL (40.65 nM) PDGF-BB and 1 mg/mL BSA over 90 minutes in 15 minute intervals. Concentration of oligonucleotides was 25 nM.

## 3.2 POLYACRYLAMIDE GEL ELECTROPHORESIS

Native polyacrylamide gel electrophoresis, native PAGE, was performed for Systems 1, 2, and 6 to show the binding and fluorescence of the aptamer strand to PDGF-BB. The expected results from the PAGE gel are shown in **Fig. 8** and the results from the PAGE gel are shown in **Fig. 9.** As **Fig. 8** illustrates, the aim of the native PAGE was to show binding of the PDGF-BB aptamers, F1 and F2, to PDGF-BB, as well as detection of the displaced partial complements, Q1, Q2, and Q6.

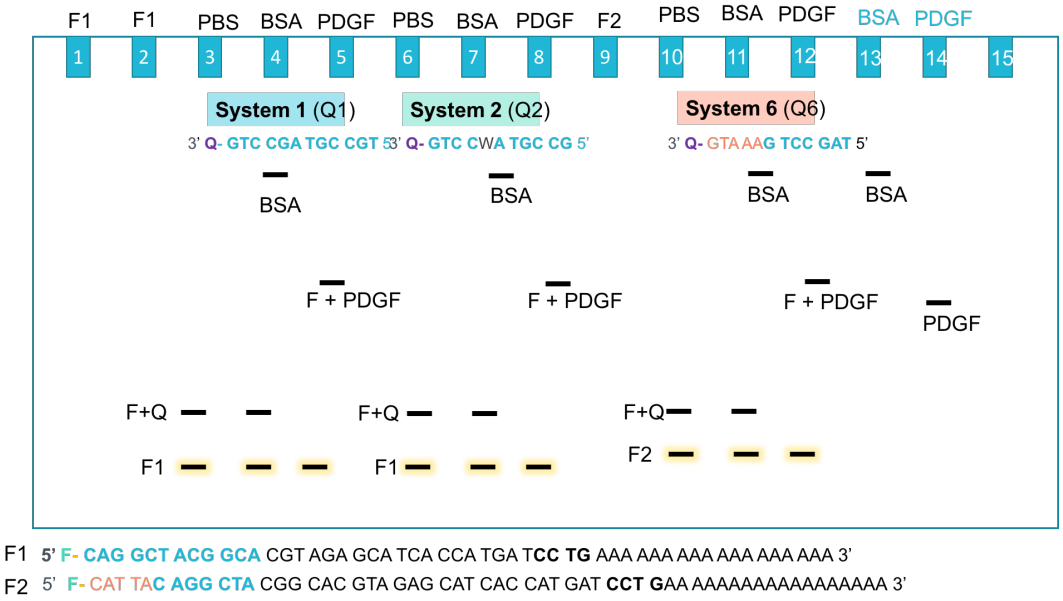


Figure 8. Depiction of expected results from native PAGE for Systems 1, 2, and 6.

However, as seen in **Fig. 9,** binding of the PDGF-BB aptamers to PDGF-BB was undetectable using the Commassie Brilliant Blue protein stain. Bands produced from BSA are indicated by arrow A. The faint bands seen in Lanes 2, 3, 6, 11and 14 is from the BSA present in the PDGF-BB solution that is added for protein stability. The bright bands located in Lanes 1, 4, 9, and 12 are from the additionally added BSA. The DNA

bands are indicated by arrow B. The bands in Lanes 3-7 are from System 6 and F2. Bands seen in Lanes 11-13 are from the complex F1 + Q1, System 1. Arrow C points toward the bands from System 2 in Lanes 8-10, and F1 in lanes 14 and 15. The DNA bands produced from System 2 (arrow C) are lower than that seen for Systems 1 and 6 (arrow B). This could be due to the inability of System 2 to fully hybridize at room temperature, thus, these bands represent only the F1 strand. The bands located in Lanes 14 and 15 (arrow C) are of the F1 strand without any partially bound complement. These bands are of the same relative migration distance on this gel. This further adds to the belief that the DNA bands seen in system 2 (arrow C) are of just the F1 strand without the Q2 complement. There is not a noticeable band shift (arrow B) between F2, (Lane 7) and the F2 + Q6 hybridized system (Lanes 3-6), System 6. However, as seen in **Fig. 9,** the gel has a noticeable 'smile effect' as the bands curve up towards the ends of the gel and sit lower in the middle. This can be caused by uneven heating of the gel during electrophoresis and prevents any slight band shifts from being visualized.

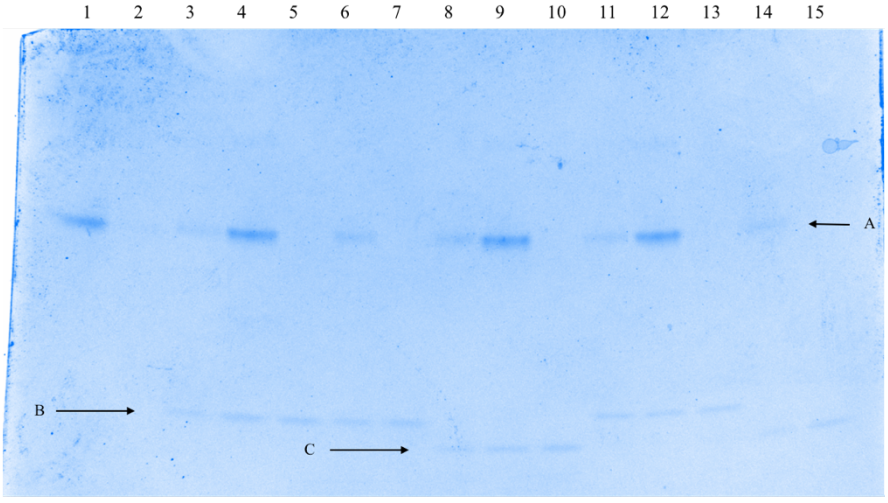


Figure 9. Native polyacrylamide gel of Systems 1, 2, and 6. All DNA concentrations are 25 μM, and PDGF-BB and BSA concentrations are 10 μg/mL. The gel was stained with Commassie Brillant Blue. Arrow A points towards bands produced by BSA. Arrows B and C point toward bands produced from the DNA complexes in Systems 1, 2 and 6.

In addition, fluorescence imaging of the gels to detect the location of the fluorophore-functionalized aptamers was unsuccessful in that no difference was seen in the location of the bands of the DNA when exposed to PBS, BSA, or PDGF, as shown in **Fig. 10**. This may have been caused by several factors including denaturation of PDGF-BB prior to gel loading, denaturation of PDGF-BB during the gel run from increased temperatures generated by the electrical current, or unbinding of the PDGF-BB aptamer from PDGF-BB caused by the electrical current of electrophoresis. Displaced partial complements, Q1, 2 and 6, were unable to be detected as they contain no secondary structure and loading enough for visualization was challenging due to their small size and low molecular weight. Lanes 3-6 show a smearing of the bands. This smearing can be caused by the degradation of the F1 strand, however, this effect is not seen in Lanes 1 or 2. This leads to the conclusion that Lanes 3-5 are visualizing both F1 and F1 + Q1. The two bands suspected of representing F1 and F1 + Q1 band are noticeably less bright than the other bands visualized on this gel. The upper bands in these Lanes, F1 + Q1 complex, are faint and could be the result of quencher presence. In Lanes 9-12 two sets of bands are again present. The lower bands have higher fluorescence intensity than the upper bands and could be indicative of quencher presence in the upper bands. However, as this upper band is also seen in Lane 9 (containing just F2 and no quenching strand) it is unlikely that this represents the System 6 complex. It is suspected that degradation of the F2 strand generated a fragment seen in the upper band.

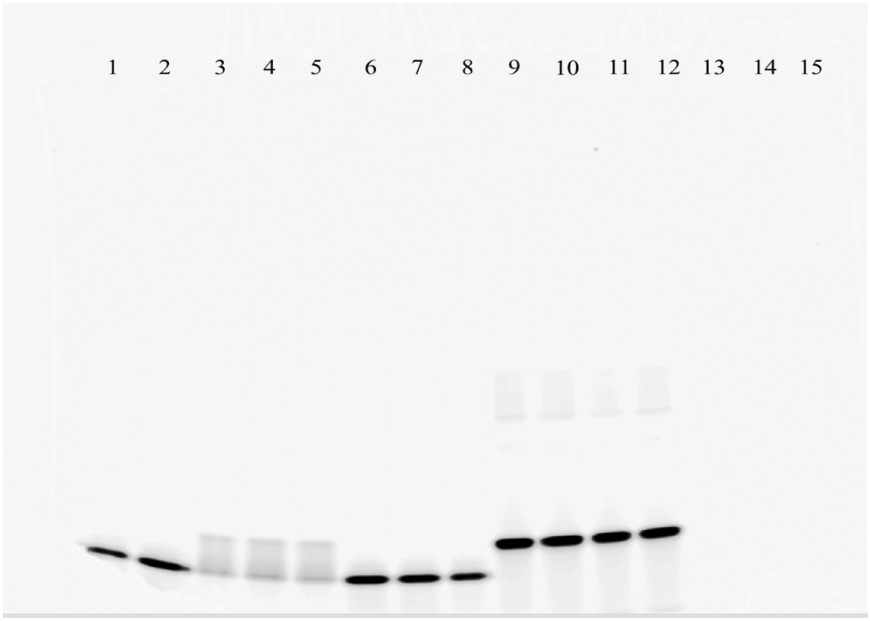


Figure 10. Native polyacrylamide gel of Systems 1, 2, and 6. All DNA concentrations are 25 μM, and PDGF-BB and BSA concentrations are 10000 ng/mL. Imaged for fluorescence using the Pharos Imager.

### 3.3 SYSTEM SELECTIVITY

To determine selectivity of Systems 1–6 to their target protein, PDGF-BB, studies were also run in the presence of vascular endothelial growth factor, VEGF, BSA, and 1% Fetal Bovine Serum, FBS. VEGF was chosen as it is a closely related protein to PDGF-BB and 1% FBS was selected as it contains many different proteins needed for the *in vitro* growth of cells, including several different growth factors. **Fig. 11** shows the fluorescence values of all systems upon interaction with PDGF-BB, VEGF, 1% FBS, and BSA.

As shown in **Fig. 11**, System 6 shows the highest rate of displacement upon exposure of PPGF-BB, and shows selectivity for PDGF-BB as it does not show an increase in fluorescence when exposed to VEGF, BSA, or 1% FBS. This is indicative of the selectivity of the fluorophore-labeled aptamer to bind only to its target, PDGF-BB.

**Fig. 12** shows the $F/F_0$ response ratio for PDGF-BB, VEGF, BSA, 1% FBS and 1% FBS + PDGF-BB for System 6.

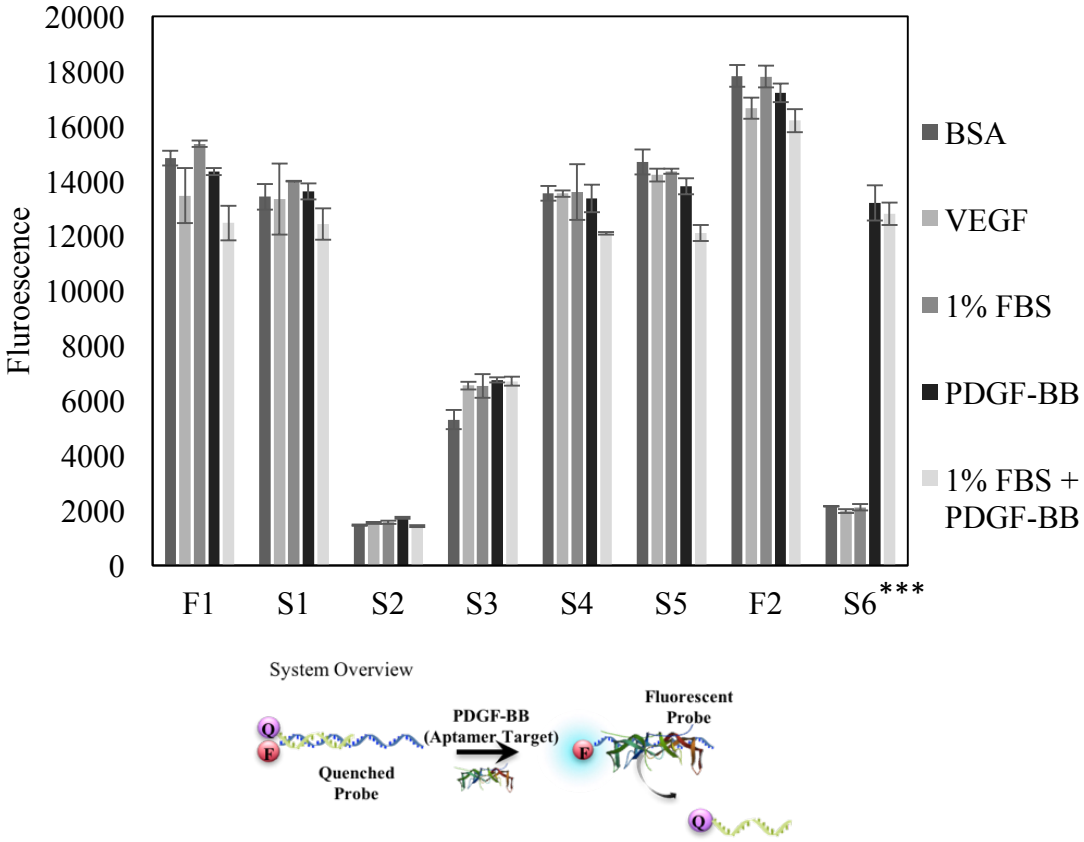


Figure 11. Selectivity of Systems 1–6, F1, and F2 towards PDGF-BB, VEGF, FBS, FBS + PDGF-BB, or BSA. All proteins were used at 1000 ng/mL while FBS was used at 1%. The average fluorescence values of each system response are displayed. Error bars represent the standard deviation between replicates (n = 3). A schematic of the partial-complement displacement upon PDGF-BB exposure leading to an increase in fluorescence is shown below the graph. *** $P \leq 0.001$.

Based on the results shown in **Fig 12,** the response ratios, $F/F_0$, were calculated using only System 6 as it was the only system to show a significant response to PDGF-BB. An $F/F_0$ value of 6.13 for PDGF-BB was calculated while the $F/F_0$ values for VEGF and 1% FBS were 0.92 and 0.98, respectively (**Fig. 12**). BSA shows a value of 1.00 as it was used as the reference, $F_0$, for the $F/F_0$ response ratio. Values close to 1, like those of VEGF and 1% FBS, indicate no displacement of the quenching strand.

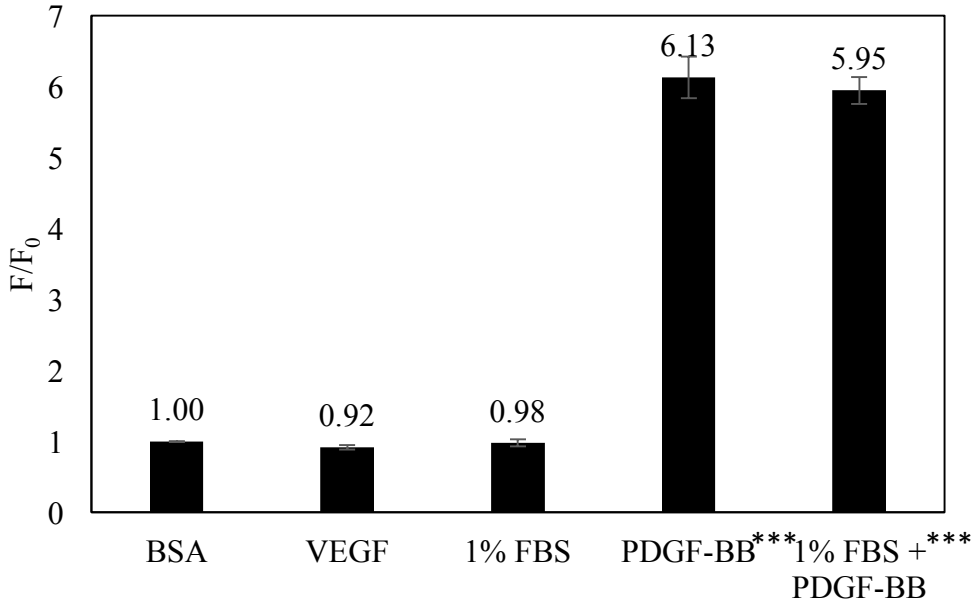


Figure 12. Selectivity of System 6 to 1000 ng/mL PDGF-BB, VEGF, and BSA, 1% FBS and 1% FBS + 1000 ng/mL PDGF-BB. The F/F0 values were calculated using BSA, F/F0=(Response to respective protein)/(Response to BSA). BSA is shown as the control with an F/F0 of 1.00. Error bars represent standard deviations between replicates (n = 3). *** $P \leq 0.001$.

### 3.4 SYSTEM SENSITIVITY

Sensitivity studies were also performed to determine the lowest concentration of PDGF-BB that each system was able to detect. The systems were run at a constant concentration of 25 nM of DNA complexes with decreasing concentrations of PDGF-BB. **Fig. 13** illustrates the detection limit of each system toward PDGF-BB. Systems 2, 4 and 5 show little initial hybridization and thus little initial quenching, which is illustrated by their fluorescent values being similar to that of the fluorophore strand, F1. System 3 demonstrates partial quenching of F1, but does not show as significant of a response to the presence of PDGF-BB as System 6. System 3 has higher initial fluorescence values and does not demonstrate as strong of a response, an increase in fluorescence, as does System 6.

System 1 shows little to no response to the presence of PDGF-BB. **Fig. 13 (B)** shows a comparison of System 1 and System 6, as well as their respective fluorophore strands, F1 and F2 to varying PDGF-BB concentrations, 500 ng/mL (20.32 nM) – 3.9 ng/mL (0.16 nM). System 6 shows an increase in fluorescence consistently beginning at 31.25 ng/mL (1.27 nM), with the most dramatic increase being from 125 ng/mL (5.08 nM) to 250 ng/mL (10.2 nM).

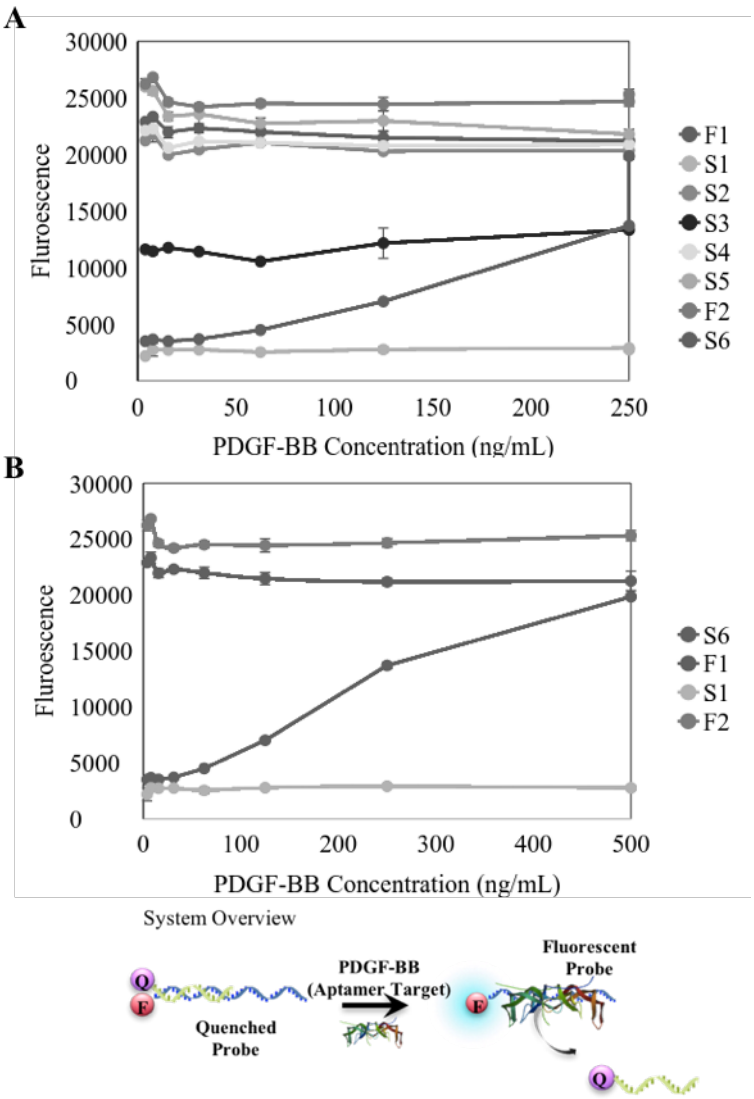


Figure 13. Sensitivity of (A) Systems 1–6, F1 and F2 (each at a concentration of 25 nM) to varying PDGF-BB concentrations, 250 ng/mL (10.16 nM) – 3.9 ng/mL (0.16 nM), and (B) Sensitivity of Systems 1 and 6, F1 and F2 to varying PDGF-BB concentrations, 500 ng/mL (20.32 nM) – 3.9 ng/mL (0.16 nM).

**Fig. 14** illustrates the response ratios of F1, F2, System 1 and System 6 to 500 ng/mL PDGF-BB (20.32 nM) from the selectivity studies performed. The response of System 6, a 6.36-fold increase in fluorescence over the fluorescence with no PDGF-BB exposure, is indicative of its ability to produce a high fluorescent signal in response to PDGF-BB, as compared to System 1, for use as FRET-sensor.

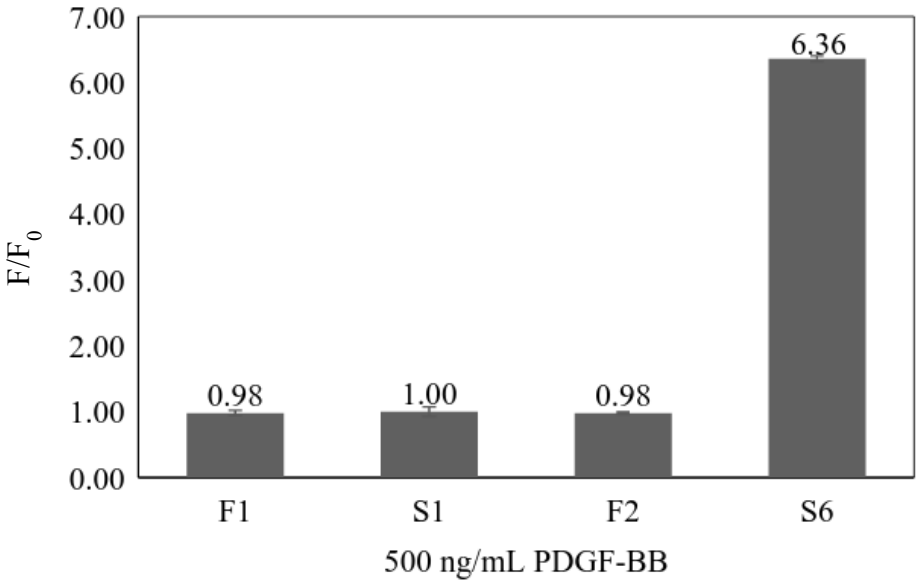


Figure 14. F/F0 response ratio of F1, F2, System 1 and System 6 to the sensitivity PDGF-BB concentration of 500 ng/mL (20.32 nM) PDGF-BB. All oligonucleotide concentrations were 25 nM.

## IV. CONCLUSIONS

The overall purpose of this research was to design and characterize a PDGF-BB aptamer-based FRET sensor that was more efficient than current generation sensors. The experiments performed in this study analyzed the efficacy, efficiency, selectivity and sensitivity of six PDGF-BB aptamer-based FRET sensors, Systems 1–6. This study utilized the previously reported system (24), System 1, as a baseline for comparison to our newly designed systems. When PDGF-BB aptamer-based FRET sensor systems bind PDGF-BB, the FRET component deactivates, leading to a fluorescence signal. When comparing System 1 to our newly designed System 6, a stronger signal is observed indicating that System 6 experiences a stronger response (**Fig. 6** and **Fig. 14**) upon interaction with PDGF-BB, thereby making it a more effective FRET-based sensor.

Fluorescence studies were performed to detect increased fluorescence of the various FRET systems in response to the target protein, PDGF-BB. Because of quencher displacement upon aptamer interaction with the target, fluorescence studies can be used to determine overall FRET sensor efficacy. Response ratios, $F/F_{0,}$ were used to display the fold increase in the fluorescence values between PDGF-BB and the BSA control. A ratio equal to 1 indicates a null response to PDGF-BB, and an $F/F_0 > 1$, is indicative of the quencher-functionalized partial complement being displaced from the fluorophore-functionalized PDGF-BB aptamer by PDGF-BB. The fluorescence assays performed with PDGF-BB and BSA show that of the six systems, System 6 has the largest response, shown by the greatest increase in fluorescence during PDGF-BB exposure and little response, minimal fluorescence increase, to the non-specific protein, BSA. The $F/F_0$ ratios calculated for all six systems show System 3, **Fig. 6**, responds slightly to PDGF-BB with $F/F_0$ values of 1.27. Systems 1, 2, 4 and 5 show $F/F_0$ values close to 1,

respectively, indicating no response to PDGF-BB.

Melting curves investigated the thermal stability of each system at their potential therapeutic temperature, physiological temperature or 37 °C, and at room temperature. The melting point temperatures of System 2, 4, and 5 could not be determined due to instrument limitations that restricted the investigation of melting curves from 5 °C to 90 °C. The previously reported system (24), System 1, was determined to possess a melting temperature of 54.5 °C as compared to the predicted 52.5 °C. While this makes System 1 stable at physiological temperatures, this high melting temperature may contribute to the low displacement levels observed in this research. For System 6, the melting point being observed at 42.5 °C was near the expected value of 40.0 °C. With a lower melting point temperature, the potential transition of System 6 into an *in vitro* or *in vivo* platform would be easier. System 6 would be stable at the physiological temperature for *in vitro* or *in vivo* studies, 37 °C, but as 37 °C nears the melting temperature of 42.5 °C, displacement by PDGF-BB would take place more readily.

Sensitivity studies done with Systems 1–6 show that response to PDGF-BB occur at concentrations of 125 ng/mL (40.65 nM) and above. The limit of detection for System 1 according to the previous report is 100 ng/mL (24). In our work, however, the detection response is over 4-fold greater with System 6 than with System 1. Consequently, we expect that the newly developed System 6 would be able to show a significantly lower limit of detection of PDGF-BB had it been run with the instrumentation utilized in the previous report.

Selectivity studies performed further demonstrated the selectivity and overall effectiveness of each system. It was important to display selectiveness of each system to

PDGF-BB, without the interference of other proteins. None of the systems studied showed any response to VEGF, BSA, or 1% FBS. System 6 showed a large response to PDGF-BB and 1% FBS + PDGF-BB, indicating no interference of aptamer binding in the presence of 1% FBS. Systems 2–5 also did not display an increased response to PDGF-BB. The response, $F/F_0$, of System 1 and System 6 during the selectivity studies were 1.01 and 6.13, respectively, when exposed to PDGF-BB, and 0.93 and 5.95 respectively when exposed to 1% FBS + PDGF-BB. The ability of System 6 (**Fig. 7)** to maintain a high fluorescence signal over 90 min is further evidence towards the affinity of the aptamer to PDGF-BB as well as usefulness of this sensor, System 6, to potentially be used as a theranostic tool.

The results of this study are important because of the enhancement to the PDGF-BB FRET sensor that it demonstrates. The ability to detect binding of the PDGF-BB aptamer to PDGF-BB, a cancer biomarker, through a detectable fluorescent signal is a vital theranostic tool. PDGF-BB's overexpression in cancer cells make it useful for targeted drug delivery systems through the use of the PDGF-BB aptamer FRET sensor (24, 32).The ability of our system, System 6, over the currently used PDGF-BB FRET sensor, System 1, to emit a significantly higher fluorescent signal upon binding allows it to be more readily detectable and provides a more confident indication of the targeted site. As these are commonly used in theranostics, certainty of target binding is critical because the drug release is based on detection of this signal (32). Our developed PDGF-BB FRET sensor, System 6, has enhanced the ability of the PDGF-BB FRET sensor to be used as a theranostic tool.

## REFERENCES


1. Kelkar, S. S.and Reineke, T.M. **2011.** Theranostics: Combining Imaging and Therapy. *Bioconjugate Chem.* 22 (10) 1879-1903.

2. Heldin, C.H. **2013.** Targeting the PDGF signaling pathway in tumor treatment. *J Cell Commun Signal.* 11, 97.

3. Yu, J., Ustach, C., Kim, H.C. **2002.** Platelet-derived Growth Factor Signaling and Human Cancer. *J Biochem Mol Bio.* 36 (1): 49-59.

4. Cao, Y., Cao, R., Hedlund, E.M., **2008.** R Regulation of tumor angiogenesis and metastasis by FGF and PDGF signaling pathways. *J Mol Med (Berl)* 86 (7): 785–789.

5. Allen, T. M. Ligand-targeted therapeutics in anticancer therapy. **2002.** *Nat. Re*V. *Cancer. 2*, 750–763.

6. Twan Lammers, Fabian Kiessling, Wim E. Hennink, and Gert Storm. **2010.** Nanotheranostics and Image-Guided Drug Delivery: Current Concepts and Future Directions. *Molecular Pharmaceutics*. *7* (6), 1899-1912.

7. Stoltenburg, R.; Reinemann, C.; Strehlitz, B. **2007.** SELEX−A (r)evolutionary method to generate high-affinity nucleic acid ligands. *Biomol. Eng*, 24, 381-410.

8. Malik, P., Katyal, V., Malik, V., Asatkar, A., Inwati, G., Mukherjee, T. **2013.** Nanobiosensors Concepts and Variations. *ISRN Nanomaterials.* 9 pages.

9. Weigum, S., Munoz, C., McIvor, E., Sutton, M., Feng, R., Cantu, T. Betancourt, T. **2016.** Targeted therapy of hepatocellular carcinoma with aptamer-functionalized biodegradable nanoparticles. *J. Nanopart. Res.* 18 (41).

10. Cheng, J., Teply, B.A., Sherifi, I., Sung, J., Luther, G., Gu. F.X., Levy-Nissenbaum, F., Radovic-Moreno, A.F., Langer, R. Farokhzad, O.C. **2007.** *Biomaterials.* 28 (5) 869-876.

11. Farokhzad, O.C., Cheng, J., Teply, B.A., Sherifi, I., Jon, A., Kantoff, P.W., Richie, J.P. Langer, R. **2006.** *Proc. Natl. Acad. Sci.* 103 (16) 6315-6320.

12. Yu, J., Ustach, C., Kim, H.C. **2002.** Platelet-derived Growth Factor Signaling and Human Cancer. *J Biochem Mol Bio.* 36 (1): 49-59.

13. Torchilin VP. Targeted pharmaceutical nanocarriers for cancer therapy and Imaging. **2007**. *AAPS J*. 9:E128–47.

14. Allam, M., Martinet, N. and Martinet, Y. **1992**. Differential migratory response of U-2 OS osteosarcoma cell to the various forms of platelet-derived growth factor. *Biochimie.* 74, 183-186.

15. Pierce, G.F., Mustoe, T.A., Altrock BW, Deuel, T.F., Thomason, A. **1991.** Role of platelet-derived growth factor in wound healing. *J. Cell. Biochem.* 45 (4): 319–326.

16. Golub, T. R., Barker, G. F., Lovett, M. and Gilliland, D. G. **1994.** Fusion of PDGF receptor beta to a novel ets-like gene, tel, in chronic myelomonocytic leukemia with t(5;12) chromosomal translocation. *Cell.* 77, 307-316.

17. Kadono, T., Kikuchi, K., Nakagawa, H. and Tamaki, K. **2000.** Expressions of various growth factors and their receptors in tissues from neurofibroma. *Dermatology* 201, 10-14.

18. Hermanson, M., Funa, K., Hartman, M., Claesson-Welsh, L., Heldin, C. H., Westermark, B. and Nister, M. **1992.** Platelet- derived growth factor and its receptors in human glioma tissue: expression of messenger RNA and protein suggests the presence of autocrine and paracrine loops. *Cancer Res.* 52, 3213-3219.

19. Nimjee, S.M., Rusconi, C.P., Sullenger, B.A. **2005.** Aptamers: An Emerging Class of Therapeutics. *Annu. Rev. Med.* 56, 555-583.

20. Pietras, K.m Sjoblom, T., Rubin, K., Heldin, C.H., Ostman, A. **2003.** PDGF receptors as cancer drug targets. *Cancer Cell.* 3 (5): 439-443.

21. Pierce, G.F., Mustoe, T.A., Altrock BW, Deuel, T.F., Thomason, A. **1991.** Role of platelet-derived growth factor in wound healing. *J. Cell. Biochem.* 45 (4): 319–326.

22. Allam, M., Martinet, N. and Martinet, Y. **1992**. Differential migratory response of U-2 OS osteosarcoma cell to the various forms of platelet-derived growth factor. *Biochimie.* 74, 183-186.

23. Kadono, T., Kikuchi, K., Nakagawa, H. and Tamaki, K. **2000.** Expressions of various growth factors and their receptors in tissues from neurofibroma. *Dermatology* 201, 10-14.

24. Li, H., Wang, M., Wang, C., Li, W., Qiang, W., Xu, D. **2013.** Silver Nanoparticle-Enhanced Fluorescence Resonance Energy Transfer Sensor for Human Platelet-Derived Growth Factor-BB Detection. *Anal. Chem.* 85 (9): 4492-4499.

25. Lin, W., Ma, G., Kampf, N., Yuan, Z.F., Chen, S. **2016.** Development of long-circulating zwitterionic cross-linked micelles for active-targeting drug delivery. *Biomacromolecules.* Epub ahead of print. PMID: 27050797

26. Ma, X., Chen, Z., Zhou, J., Weng, W., Zheng, O., Lin, Z., Guo, L., Qui, B., Chen, G. **2014.** Aptamer-based portable biosensor for platelet-derived growth factor-BB (PDGF-BB) with personal glucose meter readout. 15 (15): 412-416.

27. Huang Y, Nie XM, Gan SL, Jiang JH, Shen GL, Yu RQ. **2008.** Electrochemical immunosensor of platelet-derived growth factor with aptamer-primed polymerase amplification. *Anal Biochem*. 382,16–22.

28. Li C, Wang ZY, Gao T, Duan AP, Li GX. **2013.** Fabrication of hand-in-hand nanostructure for one-step protein detection. *Chem Commun*. 49, 3760–3762.

29. Rahman, A., Yusuf, S.W., Ewer, M.S. **2007.** Anthracycline-induced cardiotoxicity and the cardiac-sparing effect of liposomal formulation. *Int. J. Nanomedicine.* 2 (4): 567-583.

30. Lu, J., Liong, M., Zink, J.I., Tamanoi, F. **2007.** Mesoporous Silica Nanoparticles as a Delivery System for Hydrophobic Anticancer Drugs. *Small Mol*. 3, 1341-1346.

31. Nutui, R. and Li, Y. **2003.** Structure-Switching Signalling Aptamers. *J. Am. Chem Soc.* 123 (16): 4771-4778.

32. Wu X, Chen J, Wu M, Zhao JX. **2015.** Aptamers: Active Targeting Ligands for Cancer Diagnosis and Therapy. *Theranostics*. 5 (4): 322-344.

33. Owczarzy, R. Tataurov, A.V., Wu, Y. Manthey, J.A., McQuisten, K.A., Almabrazi, H.G., Pedersen, K., Lin, Y. Garretson, J., McEntaggart, N.O. **2008**. IDT ScitTools: a suit for analysis and design of nucleic acid oligomers. *Nucleic Acids Res.* 36 (2).

34. IDT OligoAnalyzer Tool, IDT, Coralville, USA. Retrieved 12 December, **2012**. http://www.idtdna.com/Scitools.

35. Green, L.S., Jellinek, D., Jenison, R., Ostman, A., Heldin, C.H., Janjic, N. **1996.** Inhibitory DNA ligands to Platelet-Derived Growth Factor B-Chain. *Biochem.* 35, 14413-14424.